Corrosion Rates of API 5L X-52 and X-65 Steels in Synthetic Brines and Brines with H₂S as a Function of Rate in a Rotating Cylinder Electrode

A. Cervantes-Tobón, J. G. Godínez-Salcedo[*], J. L. González-Velázquez, M. Díaz-Cruz

Instituto Politécnico Nacional, Departamento de Ingeniería Metalúrgica, ESIQIE, U.P. Adolfo López Mateos, Zacatenco, 07738 México, D.F., México.
[*]E-mail: drgodinez@hotmail.com

This paper investigates the importance of the hydrodynamic conditions in the corrosion rates in steel type API 5L grade X-52 and X-65 in synthetic brine with and without H₂S at 30 and 60°C, tested in a rotating cylindrical electrode (RCE) under hydrodynamic flow conditions within a rotation range of 0 to 7500 rpm (4.319 m/s). It was found that the rotation rate influences the electrochemical process which takes place in the steel surface because it increases the corrosion rate with increasing rotational rate. As expected, it was observed that at a temperature of 60°C, corrosion rates higher than the temperature of 30°C were obtained, this effect being more evident in media with H₂S. And the effect of H₂S in the steel, was the one of increasing the corrosion rate drastically as a function of the rotational rate. In the absence of H₂S, the corrosion products formed on the steel surfaces were composed mainly of iron oxides, and in brine containing H₂S the corrosion products were composed mainly of iron oxides and some sulfur (mackinawite) which was nonadherent and cracks easily. The steel has the best behavior under absence of H₂S at 30°C is the API 5L X-52 as it has the lowest values of corrosion rates not so when the temperature is increased to 60°C where the steel has the best behavior is the API 5L X-65. Under presence of H₂S at 30 and 60°C the steel has the best performance with respect to the corrosion rate by exhibiting lower values is the API 5L X-52.

1. INTRODUCTION

It is generally accepted that the corrosion rate of steel in fluid media increases with increasing flow rate, due to the mechanical removal of the passive films on the surface as well as the dissolution or delay of corrosion products growth at different flow rates. Another mechanism that explains the

greater corrosion rates at high flow conditions is erosion, especially at high flow rates where the phenomenon called erosion-corrosion takes place.

In the pipeline hydrocarbon transportation industry [1-3] the problem of flow enhanced corrosion is frequently coupled to the increased corrosion rates caused by the increasing contents of H_2S in current oil and gas production, therefore it is critical to assess the severity of corrosion as a function of the flow rate and the H_2S contents [4-7]. However there are not enough published data to predict the corrosion rates as influenced by these two factors.

The increasing need to understand the corrosion behavior of steels under turbulent flow conditions has lead some laboratories to carry out studies simulating these conditions with different degrees of success [8-10]. The use of the rotating cylinder electrode (RCE), as a hydrodynamic test system at laboratory level, has been gaining popularity in recent years [11-12].

The RCE is a useful tool for understanding the mass transfer processes, the effects or surface films, inhibition phenomena, etc. [13-15] taking place in turbulent flow conditions. This study shows the results of the measurements of the corrosion rates of type API 5L X-52 and API 5L X-65 steels in a multiphase system consisting of a brine added with kerosene and saturated with H_2S by means of a rotating cylindrical electrode (RCE) at different conditions of temperature and electrode rotation rate.

1.1. Theoretical Framework

In an oil or gas pipeline system, liquid water is separated or condensed on the walls of the pipes and then dissolves hydrogen sulfide creating the electrolytic medium, which allows the sour corrosion process to take place. The proposed dissolution reactions in this case are [16,17]:

$H_2S_{(g)} \leftrightarrow H_2S_{(ac)}$

$H_2S_{(ac)} \leftrightarrow H^+_{(ac)} + HS^{-1}_{(ac)}$

$HS^{-1}_{(ac)} \leftrightarrow H^+_{(ac)} + S^{-2}_{(ac)}$
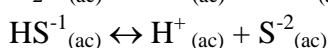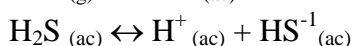
The last two reactions result from the dissolution of H_2S and represent respectively the first and second stages of dissociation of H_2S. In general:

$H_2S_{(ac)} \leftrightarrow 2H^+_{(ac)} + S^{-2}_{(ac)}$ (Overall reaction)
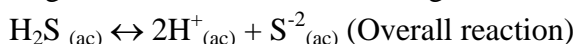
Hydrogen sulfide does induce a potential difference between heterogeneous areas of the metal, sufficient for its polarization, thus generating anodic and cathodic areas between regions near the same metal. At the anode, constituted by the same steel, the metal dissolution reaction takes place:

$Fe_{(s)} \leftrightarrow Fe_{(ac)} + 2e$ (Anode)
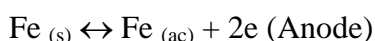
Further, the sulfide ions (HS^{-1} and S^{-2}) combine with iron to form different sulfur species (Fe_xS_y), which together with other corrosion products form a film on the metal surface in which cathodic reaction takes place: the two ions (protons) resulting from the aqueous dissociation of H_2S combine with the two electrons produced at the anode by oxidation of iron to form hydrogen atoms on the surface of steel:

$2H^+_{(ac)} + 2e \leftrightarrow 2H^°_{(ac)}$ (Cathode)

The hydrogen atoms absorbed on the surface of metal combine with each other and form molecular hydrogen gas, which appear at the surface as a form of bubbles:

$2H°_{(ac)} \leftrightarrow H_{2\,(g)}\uparrow$
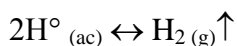
The combination of all electrochemical reactions outlined above, the following overall reaction of corrosion of steel in a medium containing H_2S results [18, 19]:

$xFe_{(s)} + y(H_2S)_{(ac)} \leftrightarrow Fe_xS_{y\,(s)} + yH_{2\,(g)}$
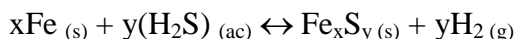
The main corrosion product formed in the surface of steel in H_2S is the ferrous sulfide (FeS), known as mackinawite [20]; however, depending on pH, partial pressure and the oxidation potential of the medium, the sulfides can take different molecular forms (eg FeS_2 or Fe_7S_8) [21].

Most of the corrosion studies of steel in H_2S have been carried out under static conditions, but in pipeline service, the corrosion occurs mainly under active flow conditions [22].

As the transfer of momentum is intensified, the rate at which chemical reactants or reaction products are transported to and from the metal surface is increased, thus increasing the corrosion rate.

The rotating cylindrical electrode (RCE) is a tool that allows to perform tests under variable flow conditions at laboratory scale that simulate a stream of corrosive fluid passing on a corroding surface [23-26].

The RCE has many advantages including: small quantities of test solution are required to perform the test [27]. The equipment is simple and of easy operation, the test is inexpensive in comparation with other tests. Several workers have used the RCE in order to determinate the influence of turbulent flow conditions on the corrosion rate [23, 28-31].

2. EXPERIMENTAL

2.1. Test Environment.

The test solution was a brine prepared according to NACE standard 1D-196 [32] with 106.5789 g/l NaCl, 4.4773 g/l $CaCl_2$ $2H_2O$, 2.061 g/l $MgCl_2$ $6H_2O$ and 10% kerosene was added. The pH was 5.98 and the test temperatures were 30 and 60ºC. Another solution was also brine prepared under the same procedure as above, except that hydrogen sulfide (H_2S) at 1387.2 ppm was added. The pH was 3.89 and the temperatures of the solutions were 30 and 60ºC. The test solutions were deaerated with nitrogen gas for a period of 30 minutes as stated in the ASTM G59-97 (Reapproved 2003) [33], to remove dissolved oxygen.

2.2. Experimental set up.

A double bottom cell made of Pyrex glass heated with hot water was used. Cylindrical tests specimens were cut off from actual pipes of 11 mm or more of thickness in the longitudinal direction. The total area exposed of the working electrode was 3.5 cm^2 for both static and dynamic tests. The reference electrode was saturated calomel electrode, and two auxiliary electrodes of sintered graphite rods were used. Before each experiment the working electrode was polished with grade 600 silicon carbide paper, cleaned with deionized water and degreased with acetone. All electrochemical tests were performed on clean recently prepared samples and fresh solutions.

2.3. Hydrodynamic conditions.

The hydrodynamic simulations of flow velocity in the laboratory were carried out at a RCE made by Radiometer Analytical, type EDI 10000 connected to a Potentiostat/Galvanostat.

The corrosion rate of the system was evaluated at different electrode rotation rates. The working electrode rotation rates used in this study were varied from 0 to 7500 rpm (4.319 m/s), with increments of 500 rpm. The selection of these ranges were based on the conditions commonly observed at industrial facilities, as well as on the values of the Reynolds numbers (Re) allowing the validation of the existent hydrodynamic and mass transfer correlations for the RCE [23-26].

2.4. Corrosion rate measurements.

For Conducting Potentiodynamic Polarization Resistance Measurements a "Standard Test Method for Conducting Potentiodynamic Polarization Resistance Measurements"[33] (ASTM G59-97 (Reapproved 2003)) was applied by means of the commercial software POWER SUIT of Princeton Applied Research by using a Potentiostat/Galvanostat Princeton Applied Research model 263A (over the range of $\pm$ 20 mV). The polarization curves were obtained at a rate of 0.166 mV per second. The corrosion rate was obtained as a function of rotation rate for the steels used in brine added with 10% of kerosene in absence and presence of H_2S at 30 and 60°C. To make the results reliable three readings were taken for each rotation rate range employed, allowing the system to stabilize for 5 minutes before running the test and retake the reading of both the potential and the corrosion rate for each of the steel used in the investigation.

2.5. SEM characterization of corrosion products.

The surface morphology and composition of the corrosion products formed on electrode surface was characterized and analyzed using a Jeol 6300 SEM and the coupled EDX.

3. RESULTS AND DISCUSSION

3.1. Chemical analysis and metallographic.

The chemical compositions (wt.%) of the steels employed are shown in Table 1.

Table 1. Chemical composition of the API 5L X-52 and X-65 steels (wt.%).

Steel	C	Mn	Si	P	S	Cr	Cu	Ni	Fe
API 5L X-52	0.111	0.955	0.175	0.005	0.022	0.037	0.293	0.013	98.3
API 5L X-65	0.154	1.357	0.231	0.023	0.014	0.061	0.001	0.022	98.0

The microstructure of both steels shown in Figures 1 and 2 depicting pearlite colonies distributed in a ferrite matrix, this is in agreement with similar microstructure obtained by others [34-36]. Table 2 shows the contents of ferrite, pearlite and grain size of the samples with the same magnification:

Table 2. Quantification of phases for steels used in the present investigation along the longitudinal section.

Steel	% Ferrite	% Pearlite	ASTM Grain
API 5L X-52	86.64	13.35	8
API 5L X-65	80.57	19.42	9
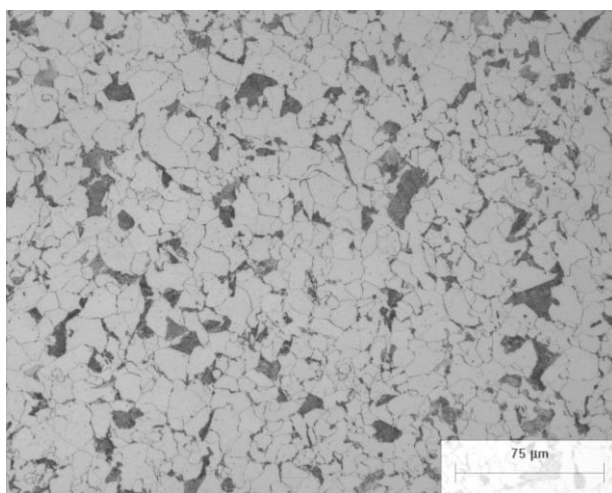
Figure 1. Microstructure of API 5L X-52 steel.
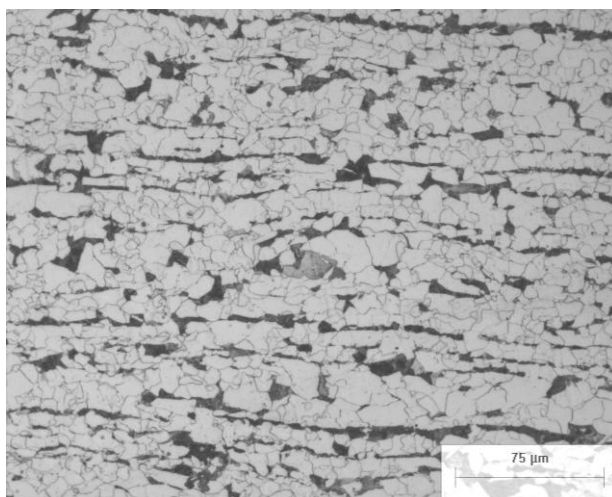
Figure 2. Microstructure of API 5L X-65 steel.

3.2. Corrosion Rate in the absence of H₂S at 30 and 60°C.

3.2.1. Steel API 5L X-52 at 30 and 60°C.

In Figure 3 the results obtained of corrosion rate as a function of rotation rate for steel API 5L X-52 in brine NACE 1D-196 are shown at 30 and 60°C. This figure shows that the corrosion rate increases with the temperature for all the flow rates, in general, the electrochemical processes of the corrosion are activated with temperature (as report H.S. Klapper et al [37] in a corrosion of UNS G10200 steel in brines under hydrodynamic conditions). Besides that the corrosion rate increases with the increment of flow rate, because, the flow increases the arrival toward the metallic surface of the reduction species and it takes away from these the species of oxidation, besides the possible erosion of corrosion products. The acceleration stages of corrosion rate as a function of rotation rate may be associated to the erosion of the layers the corrosion products. At 30°C, the corrosion rate tends to stabilize at 30 mpy for a rotation rate of 2 m/s, that which can associate to the consolidation of layers of corrosion products that this can go growing with the speed of the flow, establishing a balance with the erosion of such. At 60°C, the corrosion rates not tend to stabilize, on the contrary they tend to increase to more than 130 mpy for rotation rates of more to 1 m/s, and for what in this case the layers of the products of corrosion didn't have control about the corrosion rate. From EDX analysis it was found that both 30 and at 60°C, the corrosion products that formed were mainly oxides (FeO, Fe_2O_3, Fe_3O_4), as shown in Fig 11 (a) in the case of API 5L X-52 steel at 60°C.
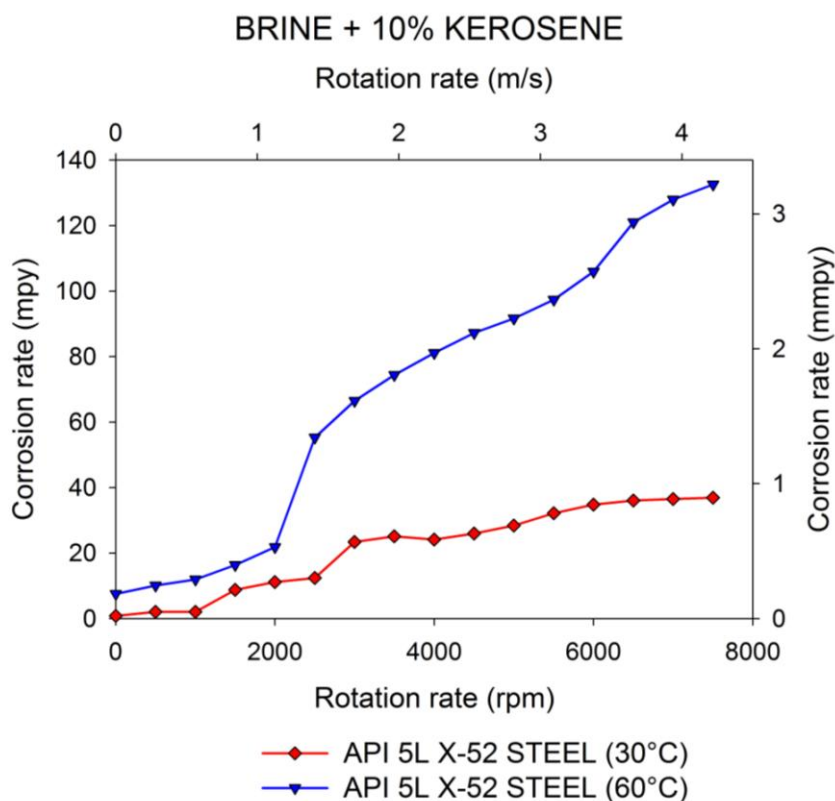
Figure 3. Corrosion rate (Cr) in function of the rotation rate for the API 5L X-52 steel in brine added with 10% kerosene in the absence of H₂S at 30 and 60°C.

3.2.2. Steel API 5L X-65 at 30 and 60°C.

For API 5L X-65 steel, Figure 4, at 30°C it was found a similar behavior for the API 5L X-52 steel, where the corrosion rates also spread to be stabilized in approximately 30 mpy for rotation rates of the order of 2 m/s. In this case the graph shows a continuous growth of a single layer of corrosion products is suggested from rotation rates from 0 to 4 m/s that stabilize the corrosion rates in 30 mpy. At 60°C in the same Figure 4, it was also found that the corrosion rates in this API 5L X-65 steel, are larger than to 30°C besides that these they spread to be stabilized and/or to diminish in approximately 80 mpy for rotating rates of the order of 4 m/s. In this case the products of corrosion were more resistant than for the steel API 5L X-52, possibly to the greatest content in carbon (cementite), Table (2), of this steel. From EDX analysis it was found that both 30 and at 60°C, the corrosion products that formed were mainly oxides (FeO, Fe_2O_3, Fe_3O_4), as shown in Fig 11 (b) for the case of API 5L-X65 steel at 60°C.
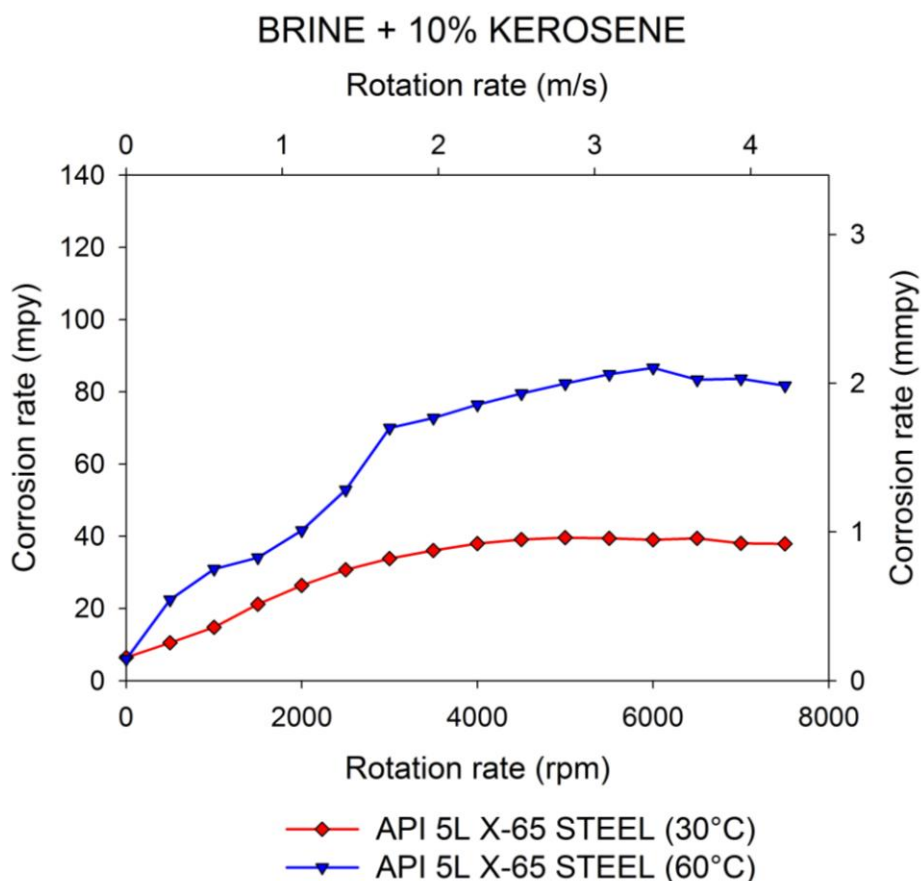
Figure 4. Corrosion rate (Cr) as a function of the rotation rate for the API 5L X-65 steel in brine added with 10% kerosene in absence of H_2S at 30 and 60°C.

3.2.3. Comparison of the corrosion rates as a function of rotation rates for steels API 5L X-52 and API 5LX-65 in brine NACE 1D-196 in the absence of H₂S at 30 and 60°C.

In the Figure 5 the results obtained of corrosion rate of steels API 5L X-52 and API 5L X-65 are compared in a brine NACE 1D-196 at 30°C, of what we can conclude that the steel API 5L X-52 presents corrosion rate assisted by flow smaller than steel API 5L X-65, because this steel contains more carbon and consequently more cementite. The cementite is more resistant to the corrosion. As the ferrite corrodes, the sheets of the cementite will arise from the surface, providing a superficial additional area for the cathodic reaction, that which increases the corrosion rate [38].
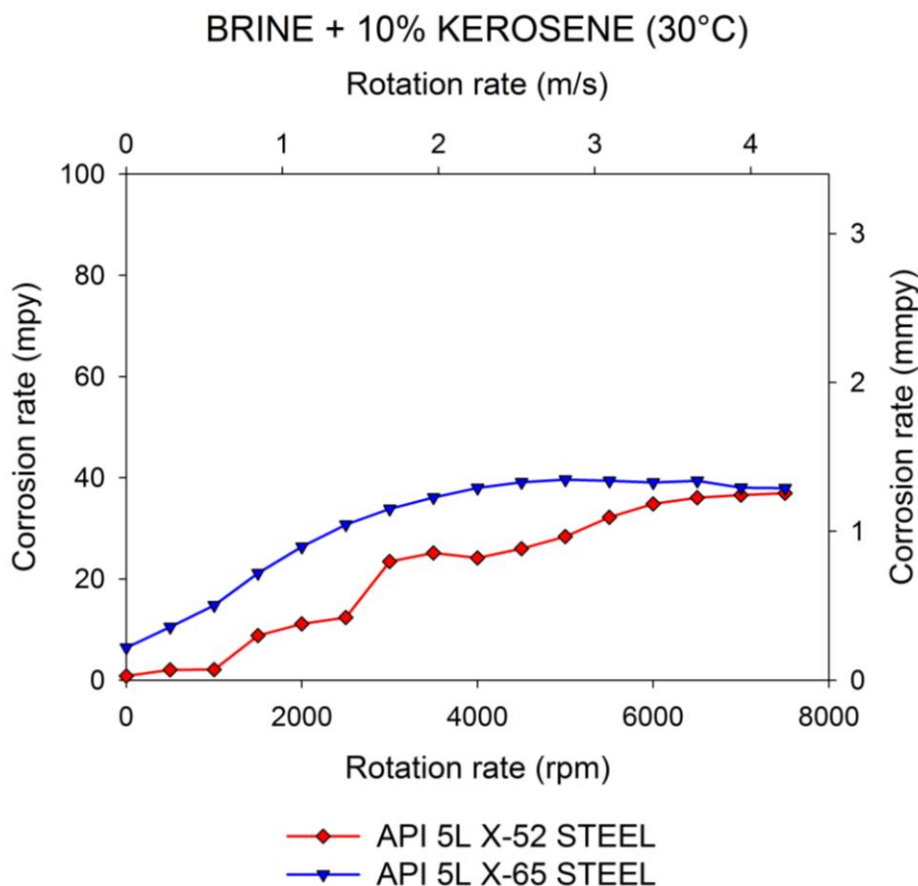
Figure 5. Corrosion rate (Cr) comparision for the API 5L X-52 and X-65 steels in brine added with 10% kerosene in absence of H₂S at 30°C.

In Figure 6, the same comparison is made from the same steels at 60°C. In this case the corrosion rates assisted by flow, for the two steels presented an alternate behavior. For rotating rates smaller than 1.5 m/s the steel API 5L X-52 presents smaller corrosion rates that the steel API 5L X-65 but flow rates more than 1.5 m/s, the steel API 5L X-52 presents more corrosion rate that the steel API 5L X-65, these corrosion rate were growing, without limit, while the corrosion rates of the steel API 5L X-65 spread to be stabilized to 80 mpy, what was possibly due to that for the rotation rates larger than 1.5 m/s the erosion of the cementite sheets and of corrosion products they are balanced with the corrosion rate of the ferrite.
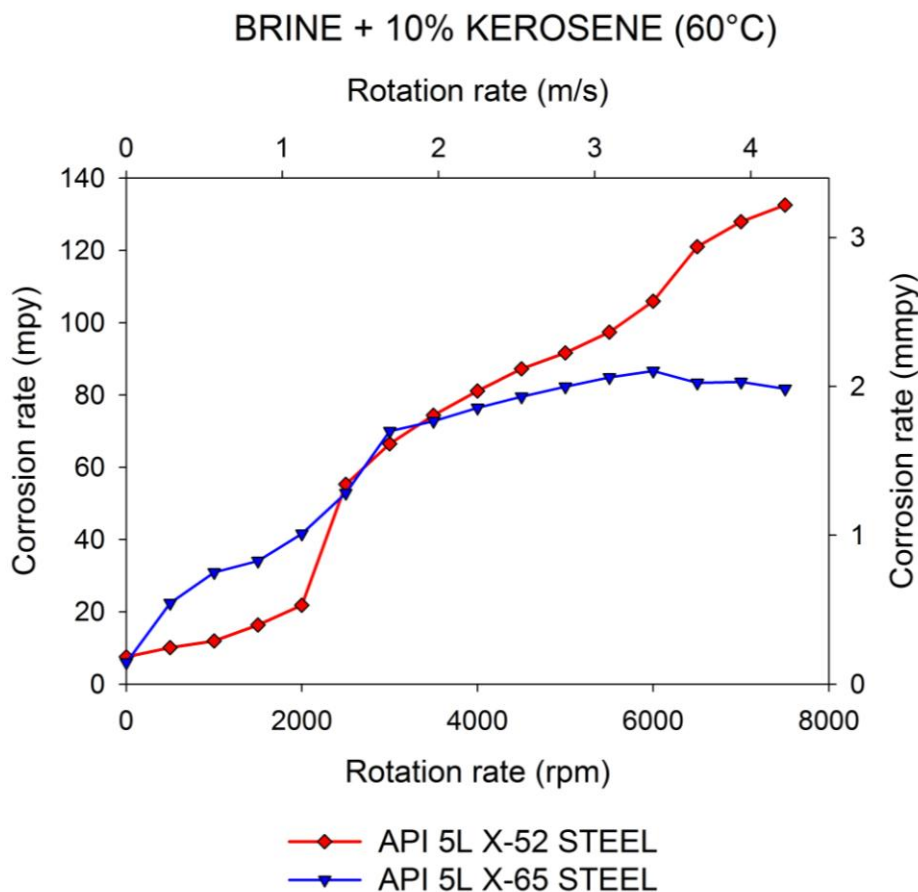
Figure 6. Corrosion rate (Cr) in function of the rotation rate comparasion for the API 5L X-52 and X-65 steels in brine added with 10% kerosene in the absence of H_2S at 60°C.

3.3. Corrosion Rate under presence of H_2S at 30 and 60°C.

3.3.1. Steel API 5L X-52 at 30 and 60°C.

In Figure 7 the results obtained of corrosion rate as a function of rotating rate in brine NACE 1D-196 whit H_2S at 30 and 60°C are shown for the steel API-5L X-52. Where can be proven that for this mean, the corrosion rate also increases with the temperature for all the rotation rates (in general, the electrochemical process of the corrosion is activated with the temperature). As seen in Figure 7, in comparison with the Figure 5, for 30°C the effect of H_2S in the steel, was the one of increasing the corrosion rate drastically as a function of the rotation rate. In this, case the corrosion rate increases monotonously from approximately 100 mpy under static conditions up to 200 mpy for rotation rates of the order of 4 m/s.
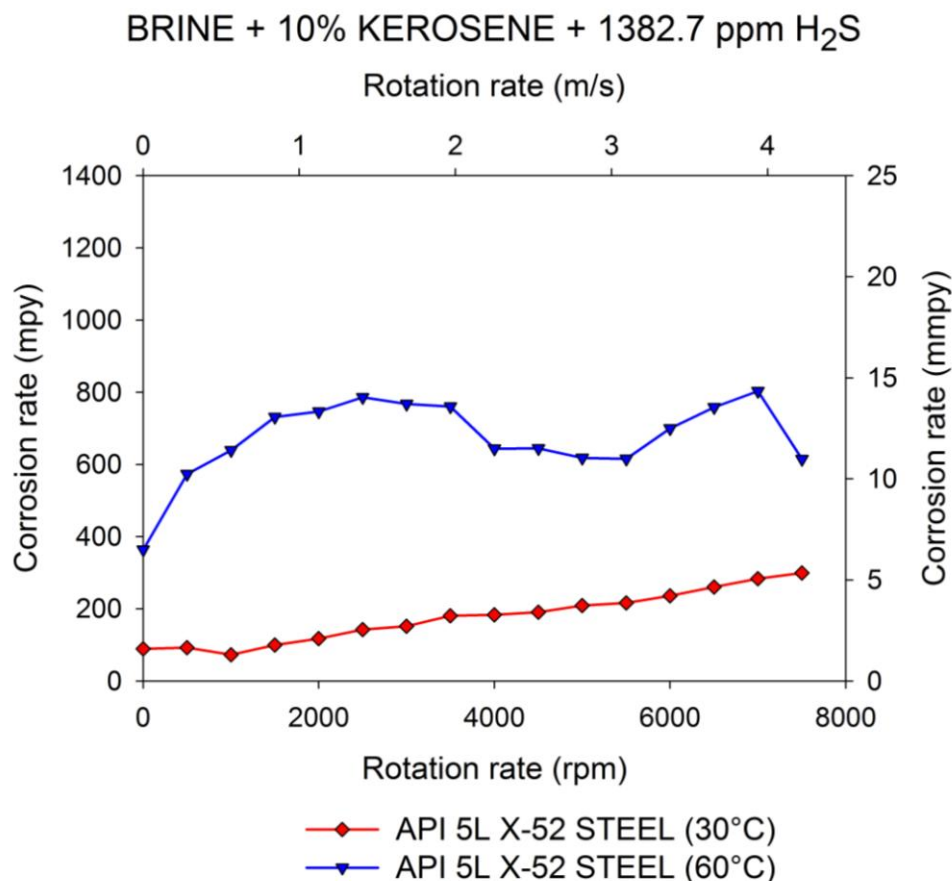
Figure 7. Corrosion rate (Cr) as a function of the rotation rate for the API 5L X-52 steel in brine added with 10% kerosene in presence of H_2S at 30 and 60°C .

This increment in the corrosion rate is due to the presence of the ions mainly H+ coming from the watery breakup of H_2S, these ions accelerate the reduction and oxidation reactions attended by the flow. Due to the monotonous growing behavior of the corrosion rate as a function of rotation rate, there are not indications of the formation of layers of corrosion products it to interfere significantly in the corrosion rate. At 60°C the effect of H_2S, in the of corrosion rate as a function of rotation rate, is even more drastic that to 30°C, like one can see of the corresponding graph no monotonous of the Figure 7.

The growth of the corrosion rate as a function of the rotation rate possibly presented maximum and minimum due to the formation and erosion, respectively, of layers of corrosion products. In this case, the corrosion products formed in addition to the oxides (FeO, Fe_2O_3, Fe_3O_4), both for 30 to 60°C due to the presence of sulfur is formed Mackinawita layer. In Figure 12 (b) shows the EDX analysis for the 60°C.

3.3.2. Steel API 5L X-65 at 30 and 60°C.

In Figure 8. The results obtained of the corrosion rate as a function of rotation rate for the API 5L X-65 steel in brine NACE 1D-196 with H_2S at 30 and 60°C are shown. For this steel type the

corrosion rates were even larger than for the steel API 5L X-52, in principle due to their microstructure and composition. In this case the effect of the temperature was not so marked, being that in three rotating rates the corrosion rate are same for 30 and 60°C and that in rotation rates ≥ 4 m/s the corrosion rates are greater at 30°C than at 60°C, indicating a tendency to fall to 60°C and a tendency to increase for 30°C. Also in both temperatures the corresponding graphs showed tendencies towards the formation and erosion of layers of corrosion products. As in the case of steel formed API 5L X-52 the same type of corrosion products, oxides (FeO, Fe_2O_3, Fe_3O_4) and Mackinawita, as seen in the EDX analysis, Figure 12 (b). For rates greater than 3.5 m/s, layer of corrosion products tend to consolidate at higher temperatures (60^oC) and provide greater protection against 30^oC where corrosion products tend to reduce the protection.
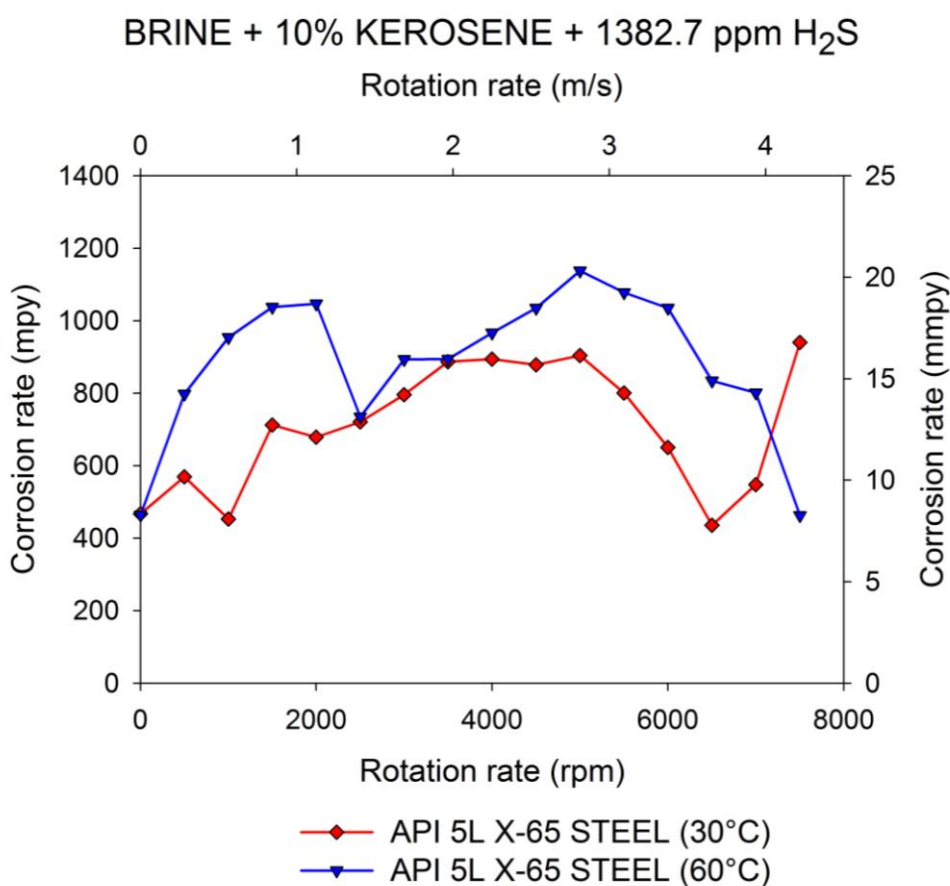
Figure 8. Corrosion rate (Cr) as a function of the rotation rate for the API 5L X-65 steel in brine added with 10% kerosene in presence of H_2S.

3.3.3 Comparison of the corrosion rates as function of rotation rates for steels API 5L X-52 and API 5L X-65 in brine NACE 1D-196 with H_2S at 30 and 60°C.

In Figure 9, the obtained results for corrosion rate as a function of rotation rate of the steels API 5L X-52 and API 5L X-65 are compared in brine NACE with H_2S to 30°C. There one can observe

that the steel API 5L X-52 presents a corrosion assisted by flow much smaller and without formation indications and erosion of layers of products of corrosion. The steel API 5L X-65 under these conditions for rotation rates ≥ 3.5 m/s presents corrosion rates with a tendency to grow to ≥ 1000 mpy. To 60°C, it Figures 10, both steels presented more corrosion rates that 30°C and for both steels according to the corresponding graphs presented formation indications and erosion of layers of products of corrosion.
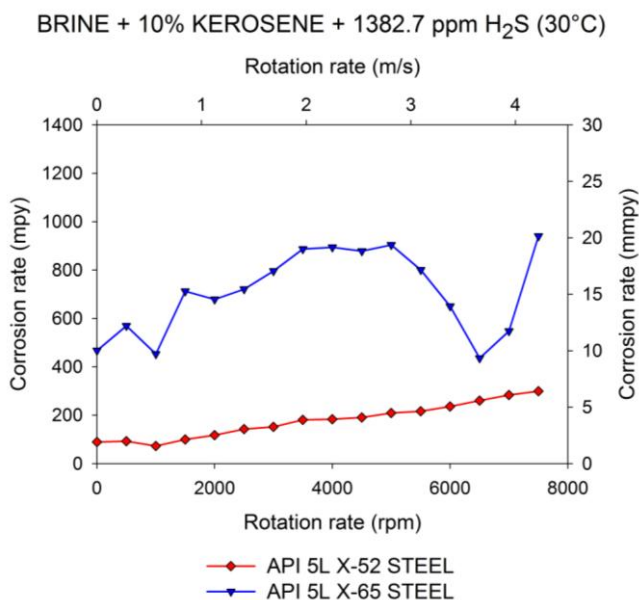
Figure 9. Corrosion rate (Cr) as a function of the rotation rate comparasion for the API 5L X-52 and API 5L X-65 steels in brine added with 10% kerosene in presence of H_2S at 30°C.
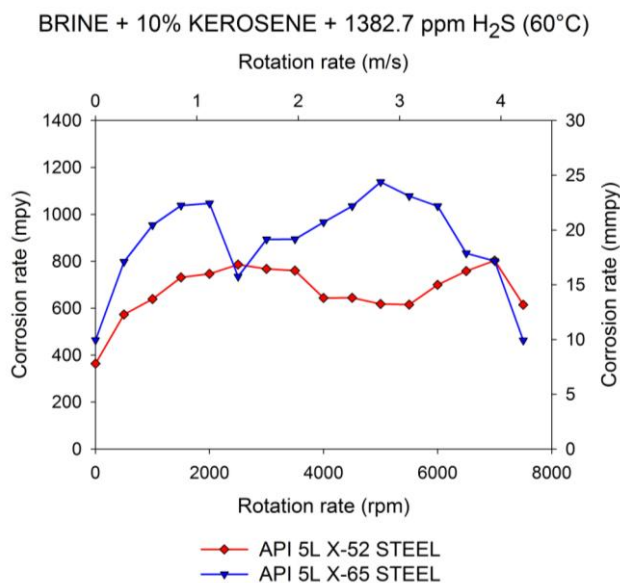
Figure 10. Corrosion rate (Cr) as a function of the rotation rate comparasion for the API 5L X-52 and API 5L X-65 steels in brine added with 10% kerosene in presence of H_2S at 60°C.

3.4. Analysis of corrosion products.
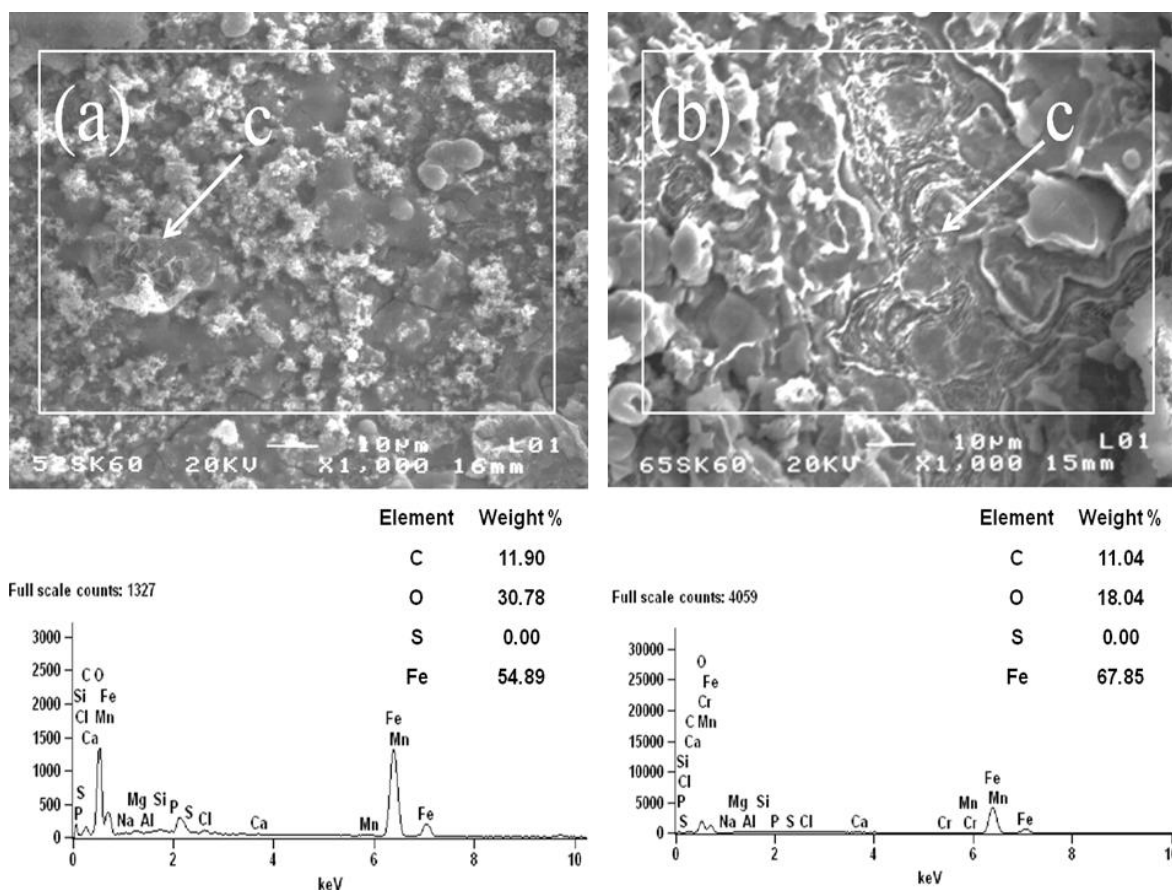
Figure 11. SEM image of corrosion products film formed on the API 5L X-52 (a) and API 5L X-65 (b) steel working electrode in brine added with 10% kerosene at 60°C in the absence of H_2S.

SEM analysis of the working electrodes exposed to synthetic brines in absence and presence of H_2S as shown in Fig. 11 and 12 respectively.

In Figure 11 EDX measurement of API 5L X-52 (a) and API 5L X-65 (b) steels in brine NACE 1D-196 at 60°C shows that the mainly identified elements are C, O, Fe. These elements on the surface indicating the presence of the protective FeO, Fe_2O_3 or Fe_3O_4 film formation (corrosion products). The presence of some oxides as Fe_2O_3 and Fe_3O_4, partially protects the steel surfaces as reported E.S. Sherif et al [39].

The arrow indicates an area (c) to be sampled so that there is also the formation of corrosion products from the same detachment due to the increasingly turbulent motion of fluid used with the rotation of the working electrode.

Figure 12. EDX measurement on API 5L X-52 (a) and API 5L X-65(b) steels in brine NACE 1D-196 at 60°C in presence of H_2S the mainly identified elements are C, O, Fe and S. Shows the film formed at the surface of the steels working electrodes. This film (corrosion products) is made from iron oxides and mackinawite (FeS_{1-x}) as reported in the literature [40-42]. It is known that H_2S contributes to the corrosion and formation of iron sulfide film.
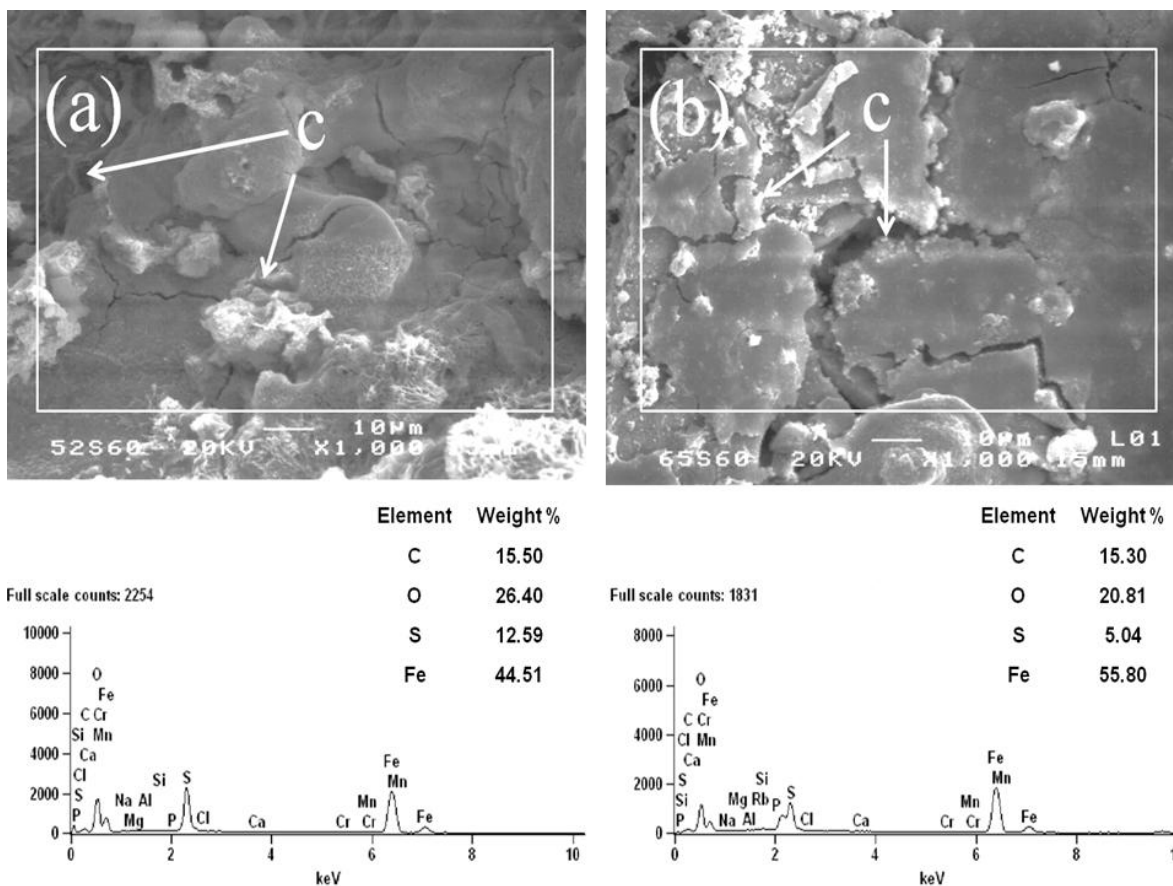
Figure 12. SEM image of corrosion products film formed on the API 5L X-52 (a) and API 5L X-65 (b) steel working electrode in brine added with 10% kerosene at 60°C in the presence of H_2S.

This film is formed almost instantaneously at the moment that the H_2S is added into the solution (brine) and has a black color, mackinawite is the first corrosion product formed at the iron/steel surface and usually forms as a precursor to other types of sulfides. The mackinawite film formed at the steel surface is nonadherent and cracks easily as shown in the figure in zone C and as reported by Shoesmith et al [43].

4. CONCLUSIONS

The electrochemical technique of linear polarization resistance used in this work shows that under turbulent flow conditions the corrosion rate is affected for both steels in corrosive media used.

The temperature also affects the corrosion rate increase with this effect being most noticeable in magnitude when this increases up to 60°C and by the addition of H_2S.

In under absence of H_2S, the corrosion products formed on API 5L-X52 and API 5L-X65 steel surfaces were composed of iron oxides (FeO, Fe_2O_3 or Fe_3O_4). The corrosion products formed on steel surfaces in brine containing H_2S at 30 and 60°C were composed of iron oxides and mackinawite, which was nonadherent and cracks easily.

Finally, we can see that the steel has the best behavior under absence of H_2S at 30°C is the API 5L X-52 as it has the lowest values of corrosion rates not so when the temperature is increased to 60°C where the steel has the best behavior is the API 5L X-65.

Under presence of H_2S at 30 and 60°C the steel has the best performance with respect to the corrosion rate by exhibiting lower values is the API 5L X-52.

References

1. Kermany, M.B. Harrop, D. BP International, SPE 29784, 1995.
2. M.S. Cayard, R.D. Kane, *Corros.*, 53 (1997) 227.
3. X.L. Cheng, H.Y. Ma, J.P. Zhang, X. C, S.H. Cheng, H.Q. Yang, *Corros.*, 54 (1998) 359.
4. H.H Hung, W.T. Tsai, J.T. Lee, *Corros.*, 52 (1996) 708.
5. R.D. Kane, "Effects of H_2S on the behaivor of Engineering Alloys: A review of literature and Experience". Hot topics, Intercorr-CLI International, Inc. Houston 1999.
6. J.A. Colwell, J.H. Payer, W.K. Boyd, CORROSION/86, 168, NACE International, Houston 1986.
7. N. Seki, T. Kotera, T. Nakasawa, CORROSION/82, 131, NACE International, Houston 1982.
8. B. Poulson, *Corros. Sci.*, 23 (1983) 391.
9. B. Poulson, *Corros. Sci.*, 35 (1993) 655.
10. B. Poulson, *J. Appl. Electrochem.*, 24 (1994) 1.
11. S. Nesic, G.T. Solvi, J. Enerhaug, *Corros.*, 51 (1995) 773.
12. S. Nesic, G.T. Solvi, J. Enerhaug, *CORROSION*/95, Paper no.130, NACE International, Houston 1995.
13. R. Galvan-martinez, J. Genesca-Llongueras, J. Mendoza-Flores, R. Duran-Romero, *CORROSION*/2003, Paper no. 03641, NACE International, Houston 2003.
14. S. Arzola-Peralta, J. Genesca-Llongueras, J. Mendoza-Flores, R. Duran-Romero, *CORROSION*/2003, Paper no.03401, NACE International, Houston 2003.
15. J. Mendoza-Flores, R. Duran-Romero, E. Garcia-Ochoa, *CORROSION*/2002, Paper no.02491, NACE International, Houston 2002.
16. S.P. Ewing, *Corros.,* 11 (1955) 51.
17. D.A. Jones, Principles and Prevention of corrosion, 2nd ed., Prentice Hall, Englewood Cliffs, NJ, 1996, 368.
18. A. G. Wikjord, T. E. Rummery, F. E. Doern, D. G. Owen, *Corros. Sci.*, 20 (1980) 651.
19. H. Ma. X. Cheng, G. Li, S. Chen, Z. Quan, S. Zhao, L. Niu, *Corros. Sci.*, 42 (2000) 1669.
20. F. H. Meyer, O. L. Riggs, R. L. McGlasson, J. D. Sudbury, *Corrosion*, 14 (1958) 69.
21. G. Schmitt, W. Bruckhoff, CORROSION, 620, NACE International, Houston, 1989.
22. T.Y. Chen, A. A. Moccari, D. D. Macdonald, *Corros.*, 48 (1992) 239.
23. D.C. Silverman, *Corros.*, 40 (1984) 220.
24. D.C. Silverman, *Corros.*, 55 (1999) 1115.
25. R.A. Holser, G. Prentice, R.B. Pond, R. J. Guanti, *Corros.*, 48 (1992).
26. L. Shreir, in: Corrosion 1, Metal/Enviroment Reactions (Eds. L.L. Shreir, R. A.. Jarman, G.T. Burstein), 3th Edition, Butterwoths, london 1994, 2:12-2:13.

27. ASTM G 170-01, "Evaluating and Qualifying Oilfield and Refinery Corrosion Inhibitors in the Laboratory", ASTM International, 1996, pp. 6-8.
28. D.C. Silverman, *J. Electrochem. Soc.*, 44 (1988) 42.
29. S. Nesic, J. Bienkowski, K. Bremhorst, K.S. Yang, *Corros.*, 56 (2000) 1005.
30. K.D. Efird, E.J. Wright, J.A. Boros, T.g. Halley, *Corros.*, 49 (1993) 992.
31. B. Poulson, *Corros. Sci.*, 23 (1983) 391.
32. NACE 1d-196: "Laboratory Test Methods for Evaluating Oilfield Corrosion Inhibitors" (Houston TX:NACE, 1996).
33. ASTM G59-97 (Reapproved 2003) "Standard Test Method for Conducting Potentiodynamic Polarization Resistance Measurements" (Houston TX:NACE, 2003).
34. R. Dong, I. Sun, Z. Liu, X. Wang and Q. Liu, *Journal of Iron and Steel Research International*, 15 (2008) 71
35. D. Clover, B. Kinsella, B. Pejcic and R. De Marco, *Journal of Applied Electrochemestry*, 35 (2005) 139.
36. C.W. Du, X.G. Li, P. Liang, Z.Y. Liu, G.F. Jia and Y.F. Cheng, *Journal of Materials Engineering and Performance,* 18 (2009) 216.
37. H.S. Klapper, D.Laverde, C. Vázquez, *Corros. Sci.*, 50 (2008) 2718.
38. E. Gulbrandsen, R. Nyborg, Trine Loland, K. Nisancioglu, *CORROSION/*2000 No. 23, (Houston, TX: NACE, 2000).
39. El-Sayed M. Sherif, Abdulhakim A. Almajid, Khalil Abdelrazek Khalil, Harri Junaedi and F.H. Latief, *Int. J. Electrochem. Sci.*, 8 (2013) 9360.
40. P.R. Rhodes, Corr. Sci., 57 (2001) 923.
41. I. Hamada and K. Yamauchi, *Metall. Mater. Trans. A Phys. Metall. Mater. Sci.*, 5 (2010) 56.
42. CH. Ren, D. Liu, Z. Bai and T. Li, *Mater. Chem. Phys.*, 93 (2005) 305.
43. D.W. Shoesmith, P. taylor, M.G. Bailey, D.G. Owen, *J. Electrochem. Soc.*, 127 (1980) 5.